Biophysical Journal
Article

Biophysical Society

Bilateral Spontaneous Otoacoustic Emissions Show Coupling between Active Oscillators in the Two Ears

Yuttana Roongthumskul,[1] Dáibhid Ó Maoiléidigh,[1,2] and A. J. Hudspeth[1,*]
[1]Howard Hughes Medical Institute and Laboratory of Sensory Neuroscience, The Rockefeller University, New York, New York and
[2]Department of Otolaryngology-Head and Neck Surgery, Stanford University School of Medicine, Stanford, California

ABSTRACT Spontaneous otoacoustic emissions (SOAEs) are weak sounds that emanate from the ears of tetrapods in the absence of acoustic stimulation. These emissions are an epiphenomenon of the inner ear's active process, which enhances the auditory system's sensitivity to weak sounds, but their mechanism of production remains a matter of debate. We recorded SOAEs simultaneously from the two ears of the tokay gecko and found that binaural emissions could be strongly correlated: some emissions occurred at the same frequency in both ears and were highly synchronized. Suppression of the emissions in one ear often changed the amplitude or shifted the frequency of emissions in the other. Decreasing the frequency of emissions from one ear by lowering its temperature usually reduced the frequency of the contralateral emissions. To understand the relationship between binaural SOAEs, we developed a mathematical model of the eardrums as noisy nonlinear oscillators coupled by the air within an animal's mouth. By according with the model, the results indicate that some SOAEs are generated bilaterally through acoustic coupling across the oral cavity. The model predicts that sound localization through the acoustic coupling between ears is influenced by the active processes of both ears.

INTRODUCTION

One of the hallmarks of auditory systems in all classes of tetrapods is the ability of inner ears to produce oscillations in the absence of external acoustic stimulation. Owing to the reverse transmission of sound through the middle ear, these oscillations elicit vibrations of the eardrum that are detected externally as weak sounds termed spontaneous otoacoustic emissions (SOAEs). From species to species, animal to animal, and ear to ear, these emissions vary in number, level, and frequency (1–5).

SOAEs are sensitive to several types of manipulation. For example, the application of a pure-tone acoustic stimulus usually attenuates an emission and causes a shift in its frequency away from that of the stimulus frequency (3,6). More rarely, emissions are enhanced or shifted toward the stimulus (7). Decreasing the body temperature evokes a decline in the frequency of emission (5,8). Finally, altering the air pressure in the ear canal strongly affects SOAEs: extreme pressure changes typically attenuate the emissions. The associated shifts in SOAE frequency are complex and vary widely between species (9–11). In addition to altering the acoustic impedance of the middle ear, changes in ear-canal pressure might influence the intracochlear noise level or the active process underlying the emissions (10–12).

Several studies report SOAEs emanating at nearly identical frequencies from both ears of an animal (13,14). In mammals, the correlations between ears are speculated to arise from efferent control owing to the medial olivocochlear system. In amphibians, binaural SOAEs are attributed to acoustic coupling between the ears (15) because in most nonmammalian tetrapods, the Eustachian tubes that connect the middle ears to the oral cavity are widely open. An external sound impinging on one tympanum can accordingly traverse the oral cavity and stimulate the contralateral ear (16–18).

Acoustic coupling between ears through the mouth yields a difference in the response amplitudes of the two eardrums; this difference might facilitate the localization of sound sources by amphibians and reptiles, including some birds (16,19,20). Whether the active process that drives SOAEs affects this mechanism for sound localization is unknown.

Submitted November 6, 2018, and accepted for publication February 28, 2019.

*Correspondence: hudspaj@rockefeller.edu

Yuttana Roongthumskul and Dáibhid Ó Maoiléidigh contributed equally to this work.

Yuttana Roongthumskul's present address is Department of Physics, Faculty of Science, Chulalongkorn University, Bangkok, Thailand.

Editor: Brian Salzberg.

https://doi.org/10.1016/j.bpj.2019.02.032

To evaluate the possibility that bilateral emissions at similar frequencies signify acoustic coupling between the two ears, we adapted a model of nonlinear, active hair cells to inquire whether airborne coupling allows the simulated emissions to entrain one another. The dynamics of coupled active oscillators has been studied extensively for many different types of coupling and continues to be a topic of intense interest (21–24). Coupling can cause effects such as synchronization, oscillation death, and multistability. Using a damped wave equation to describe the air in the oral cavity, we modeled two noisy, coupled oscillators representing the eardrums. After examining the effects of specific perturbations on emissions, we compared the model's behavior with the results of binaural recordings from the tokay gecko, a convenient experimental preparation with robust SOAEs (Fig. 1, *A* and *B*).

METHODS

Modeling coupled nonlinear oscillators

We represent the oral cavity of a tokay gecko as a closed cylinder of length L, whose ends terminate in two eardrums of area A, each connected to an SOAE generator in the inner ear (Fig. 1, *C* and *D*). Because the mouth remained slightly open during experiments, the oral cavity might be described by two half-open cylinders closely apposed at their open ends. Near the fundamental frequency of the two-cylinder system, however, the eardrums move in antiphase, as does the pressure for the fundamental mode of a cylinder closed at both ends, which motivates us to model the oral cavity as a closed cylinder. In addition, the harmonic frequencies of the head are much lower than that of a cylinder with a length equal to the head's width (25). The effective length L is chosen so that, in agreement with experimental observations, the eardrums' phase difference exhibits a shift of 180° between 3.5 and 4.0 kHz (Fig. 2 *C*).

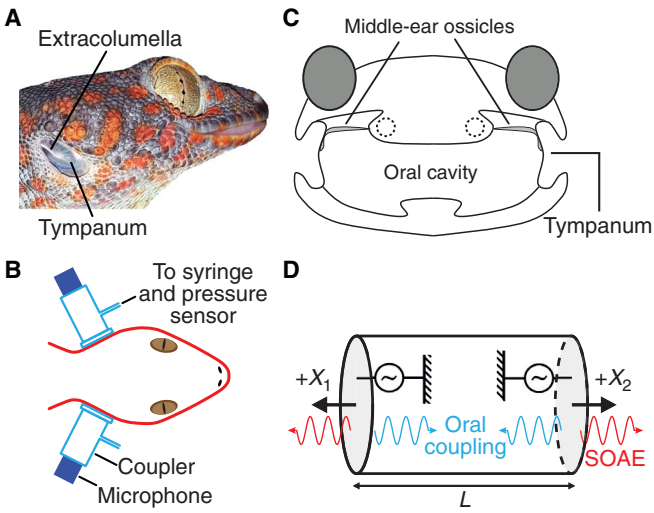

FIGURE 1 (*A*) The tympanum and the lateral articulation of the middle-ear ossicle, the extracolumella, are apparent through the tokay gecko's shallow ear canal. (*B*) A plastic coupler was sealed over each ear canal with vacuum grease. The coupler was attached to a sensitive microphone and connected by a plastic tube to a 5 mL syringe and pressure sensor. (*C*) A schematic drawing of a gecko's head shows that the two eardrums are connected through the oral cavity. Dashed circles indicate the locations of the inner ears. (*D*) In a model of the ears as two coupled nonlinear oscillators, a closed cylinder representing the oral cavity has both ends covered by eardrums, each directly connected to an active inner ear. The coordinate system is such that the positive direction corresponds to an outward motion of each eardrum. The standard parameter values used in the model are summarized in Table S1. Parameter values that differ from these standards are provided in the relevant figure captions.

The equation of motion of the nonlinear oscillator used to describe an eardrum's displacement (12) is

$$\gamma_j \frac{dx_j}{dt} = a_j\left(x_j - c_j f_j\right) - N_j\left(x_j - c_j f_j\right)^3 - K_j x_j + \left(p_j - p_{ej}\right)A + \eta_{xj}, \tag{1}$$

in which x_j denotes the displacement of the j^{th} oscillator ($j = 1, 2$). The positive direction corresponds to the displacement of each eardrum away from the midline of the head (Fig. 1 *D*). The oscillator is driven by the difference between the external pressure denoted by p_{ej} and the internal pressure p_j representing the pressure at the location of the j^{th} eardrum: $p_1 = p(0)$ and $p_2 = p(L)$. The first three terms on the right-hand side of the equation represent dynamics driven by active hair-bundle motility. The parameters a_j and K_j are stiffnesses, c_j is a compliance, γ_j is a damping coefficient, and N_j controls the strength of the system's nonlinearity. f_j is an active force whose dynamics are given by

$$\tau_j \frac{df_j}{dt} = b_j x_j - f_j + \eta_{fj}, \tag{2}$$

in which τ_j represents the timescale of the active process and b_j is a stiffness. The Gaussian white noise terms η_x and η_f satisfy

$$\begin{aligned} \langle \eta_{xm}(t) \rangle &= 0, \quad \langle \eta_{xm}(t)\eta_{xn}(t') \rangle = 2k_B T \gamma_m \delta(t-t')\delta_{m,n}, \\ \langle \eta_{fm}(t) \rangle &= 0, \quad \langle \eta_{fm}(t)\eta_{fn}(t') \rangle = 2k_B T_f b_m \tau_m \delta(t-t')\delta_{m,n}, \end{aligned} \tag{3}$$

in which k_B is the Boltzmann constant. For an active system, the effective temperature T_f may differ from the thermodynamic temperature T (26).

The motion of the air inside the cylinder is described in one dimension by its axial particle velocity $u(x, t)$ and pressure $p(x, t)$ with respect to a reference state of zero velocity, pressure $P_r = 101$ kPa, and temperature $T = 25°\text{C}$. The air dynamics is described by the noisy acoustic telegraph equations

$$\frac{\partial p(x,t)}{\partial x} = -\rho\left(R_V u(x,t) + \frac{\partial u(x,t)}{\partial t}\right) + \eta_V, \tag{4}$$

$$\frac{\partial u(x,t)}{\partial x} = -\beta\left(R_T p(x,t) + \frac{\partial p(x,t)}{\partial t}\right) + \eta_T$$

R_V and R_T are the viscous damping rate and the thermal damping rate, respectively. ρ is the air's reference density, and β is its adiabatic compressibility. The boundary conditions restrict the velocities of particles at both ends of the cylinder to equal those of the eardrums. The noise terms η_V and η_T satisfy

$$\begin{aligned} \langle \eta_V(t,x) \rangle &= 0, \\ \langle \eta_V(t,x)\eta_V(t',x') \rangle &= 2k_B T \rho R_V A^{-1} \delta(t-t')\delta(x-x'), \\ \langle \eta_T(t,x) \rangle &= 0, \\ \langle \eta_T(t,x)\eta_T(t',x') \rangle &= 2k_B T \beta R_T A^{-1} \delta(t-t')\delta(x-x'). \end{aligned} \tag{5}$$

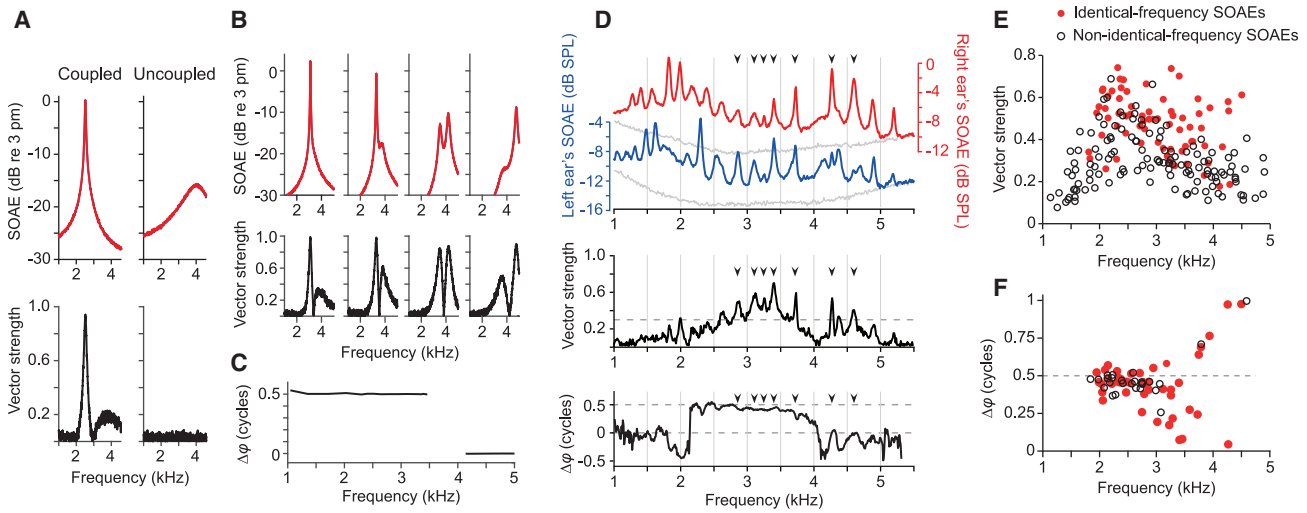

FIGURE 2 Identical-frequency SOAEs. Model: (*A*) coupling the oscillators to the oral cavity reduces their oscillation frequency and increases their amplitude. Peaks in the vector strength at the oscillation frequency indicate synchronization at that frequency. The timescale parameter $TS = 2$. (*B*) The spectra and vector strengths of two identical oscillators are shown as their peak frequency is raised by reducing the timescale parameter: left to right, $TS = 2.0, 1.5, 1.4, 1.3$. When the peak frequencies are near the fundamental frequency of the oral cavity (3.7 kHz), the acoustic coupling can create two spectral peaks. (*C*) The phase difference between two coupled identical oscillators at their largest spectral peak is shown as a function of the peak frequency, which is set by adjusting the timescale parameter from 1.25 to 5.00. The oscillators move in antiphase below the fundamental frequency but in phase above the fundamental. The largest peaks do not appear close to the fundamental frequency. Experiment: (*D*) the spectra of SOAEs recorded simultaneously from the left ear (*blue*) and right ear (*red*) display several identical-frequency SOAEs, defined by a difference of less than 10 Hz in their center frequencies. The vector strength peaks at the frequencies of some SOAEs from both ears. Black arrowheads label the identical-frequency SOAEs with vector strength exceeding 0.3. The mean phase difference between binaural SOAEs peaks is close to 0.5 cycles below 3.5 kHz and is 0 cycles above 4 kHz. When the vector strength is small (<0.3), the phase difference is not constant and fluctuates considerably around the mean. The noise floors of the spectra (*gray lines*) were obtained from the same animal after euthanasia. (*E*) Most identical-frequency SOAEs (*red dots*) possess vector strengths exceeding 0.3. The vector strength sometimes exceeds 0.3 for non-identical-frequency peaks (*black circles*). (*F*) The phase difference between most identical-frequency SOAEs whose vector strength exceeds 0.4 is close to 0.5 cycle when the frequency is less than 3 kHz and is 0 cycles, or equivalently one cycle, when the frequency exceeds 4 kHz. The data in (*E*) and (*F*) were obtained from 20 geckos.

Numerical simulations of Eqs. 1, 2, 3, 4, and 5 were performed by the forward Euler-Maruyama method (Eqs. 1 and 2) and through finite differences (Eq. 4). To decrease the computational time, the small noise terms in Eq. 4 were set to zero but are shown here for completeness. The solutions described the displacement of the eardrums x_j. The emission frequency was identical to that of the oscillator, and the emission level was defined to be the displacement of the oscillator with respect to the reference level of 3 pm, a displacement chosen to match the velocity of the eardrum at 1 kHz and 0 dB sound-pressure level (SPL) (16,27). The steady-state time traces generated by the model were analyzed in the same fashion as the experimental time traces.

Other sources of dissipation in the actual system, such as the intricate anatomy of the oral cavity and the presence of oral fluids, were accommodated through the use of damping rates larger than those corresponding to an unobstructed cylindrical cavity. More complex results could also arise from the interactions between SOAEs within an individual ear.

To change the frequency of an oscillator without changing its oscillation amplitude significantly, we used a dimensionless timescale parameter TS to rescale the oscillator's time in Eqs. 1 and 2. Conversely, to change the amplitude with little change in the frequency, we employed the dimensionless parameter DS to rescale the oscillators' displacement. These changes were achieved by rescaling the oscillators' parameters as a_j/TS^2, b_j/TS^2, K_j/TS^2, c_jTS^2, γ_j/TS, $N_j/(TS^2DS^2)$, and τ_jTS. The values of all parameters are summarized in Table S1.

Structure of the gecko's auditory system

The external ear of the tokay gecko consists of a shallow ear canal terminating in a conical tympanum whose tension is maintained by the single middle-ear ossicle, the columella, which attaches to the eardrum through a process termed the extracolumella (Fig. 1 *A*). Each internal ear includes a complex sensory epithelium, the basilar papilla, ~2 mm in length. The basal 700 μm of the organ is devoted to the frequency range 150–1000 Hz and includes some 200 hair cells (28). The more apical 1300 μm of the basilar papilla, which represents frequencies from 1 kHz to more than 5 kHz (29), supports two strips of hair cells. Beneath a narrow, continuous tectorial membrane lie 1000–1300 hair cells in rows of six to eight cells abreast; under 170 distinct sallets, there are 800–900 hair cells in rows of five to seven cells abreast (28,30).

Measurement and manipulation of SOAEs

All experimental protocols were approved by the Animal Care and Use Committee of the Rockefeller University. Young adult tokay geckos (*Gekko gecko*) of both sexes were anesthetized with an intraperitoneal injection of 20 mg/kg sodium pentobarbital (Nembutal; Akorn Pharmaceuticals, Lake Forest, IL). The body temperature of the animal was maintained by a heating pad at 28.5°C; the corresponding oral temperature was 24–25°C. For all experiments, the distance between the tips of the upper and lower jaws was maintained near 10 mm.

Measurements of SOAEs were performed inside a sound-attenuation chamber with two microphones (ER-10B+; Etymotic Research, Elk Grove Village, IL), each connected to a 20-mm-long plastic coupler. The other end of each coupler was sealed around an animal's outer ear with vacuum grease (DC-976; Dow Corning, Midland, MI). The air pressure inside each coupler was manually manipulated with a 5 mL syringe connected to the coupler by a plastic tube. The pressure level was monitored with a digital manometer (475-1-FM; Dwyer Instruments, Michigan City, IN). Because the coupler changes the acoustic-impedance load on the ear, the SOAE spectrum is expected to differ from that of an unenclosed ear. Most SOAE peaks should

increase with decreasing coupler volume and might shift in frequency, as evidenced by comparisons with spontaneous eardrum vibrations (31).

To reduce the temperature of an inner ear, we used a probe consisting of a 1.8-mm-diameter copper wire with one end attached to the cool surface of a Peltier cell (CP08; Laird Technologies, Chesterfield, MO). The other end of the wire was inserted into the mouth and gently pressed against the mucosa overlying the ventral surface of the periotic bone of the left ear. The local temperature in the vicinity of each inner ear was monitored with a thermocouple placed against the mucosa abutting the periotic bone near the Eustachian tube.

Calculation of SOAE spectra and peak detection

The pressure signal obtained from each ear was acquired from 100 s recordings in nonoverlapping 100 ms segments at a sampling interval of 20 μs. The maximal pressure levels in each window and their SDs were calculated. To exclude extreme pressure variations owing to the animal's respiratory movements, any sample whose peak pressure exceeded thrice the SD was excluded from further analysis. A finite-time Fourier transform with a Hanning window was calculated for each of the remaining sections. The SOAE amplitude spectrum was obtained by averaging the magnitudes of the spectra.

Detection of SOAE peaks was performed on a smoothed emission spectrum with a five-point moving average. A peak was defined as a point in the spectrum whose magnitude exceeded those of the adjacent troughs by more than 45 nPa, which was equivalent to a peak of 0.2 dB above the noise floor at −20 dB SPL. This criterion was chosen such that the algorithm could detect a small SOAE superimposed upon another peak. The amplitudes of the average emission spectra at the frequency corresponding to the peak were required to differ statistically from those at both adjacent troughs by a Student's t-test with a criterion of $p < 0.2$. This weak test prevented the exclusion of neighboring peaks with very close frequencies, which were often more clearly distinguished after a pressure or temperature perturbation.

The phase difference of the binaural pressure signals was extracted from the finite-time Fourier transforms of each pair of nonoverlapping 100-ms windows. The argument of a complex number Z is defined as $\phi \equiv \tan^{-1}(Im(Z)/Re(Z)) + (\pi/2)sign(Im(Z))(1 - sign(Re(Z)))$. For each frequency component, the phase difference $\Delta\phi_j(f)$ between the complex Fourier components from both ears was given by the argument of the ratio $\tilde{F}_j(f) = \tilde{F}_{j,L}(f)/\tilde{F}_{j,R}(f)$, in which $\tilde{F}_{j,L}(f)$ and $\tilde{F}_{j,R}(f)$ denote the complex Fourier component of the j^{th} segment of the signal from the left and right ear at frequency f. The phase difference of the mean $\Delta\phi(f)$ was then obtained from the argument of the quantity $\langle e^{i\Delta\phi_j(f)}\rangle$, in which $\langle\ldots\rangle$ denotes the ensemble average over all segments.

The vector strength was calculated as $V = |\langle e^{i\Delta\phi_j(f)}\rangle| = |\langle(\tilde{F}_{j,L}(f)/\tilde{F}_{j,R}(f))/|\tilde{F}_{j,L}(f)/\tilde{F}_{j,R}(f)|\rangle|$. For perfectly phase-locked signals, the phase difference is time invariant, and the vector strength becomes unity. If two emissions are independent, the phase difference varies considerably with time, and the vector strength is zero. Because the variance of the phase is high when the vector strength is low, the phase difference of the mean $\Delta\phi(f)$ is meaningful only when the vector strength is large. We found that a threshold of 0.3 was sufficient to detect the effects of excessive static pressure on the SOAE spectra (Fig. 3 *E*). Because 1000 pairs of spectra were used to calculate the vector strength, a Rayleigh test statistically resolved very small degrees of phase-locking between the eardrums (p-value $< 10^{-39}$) (32).

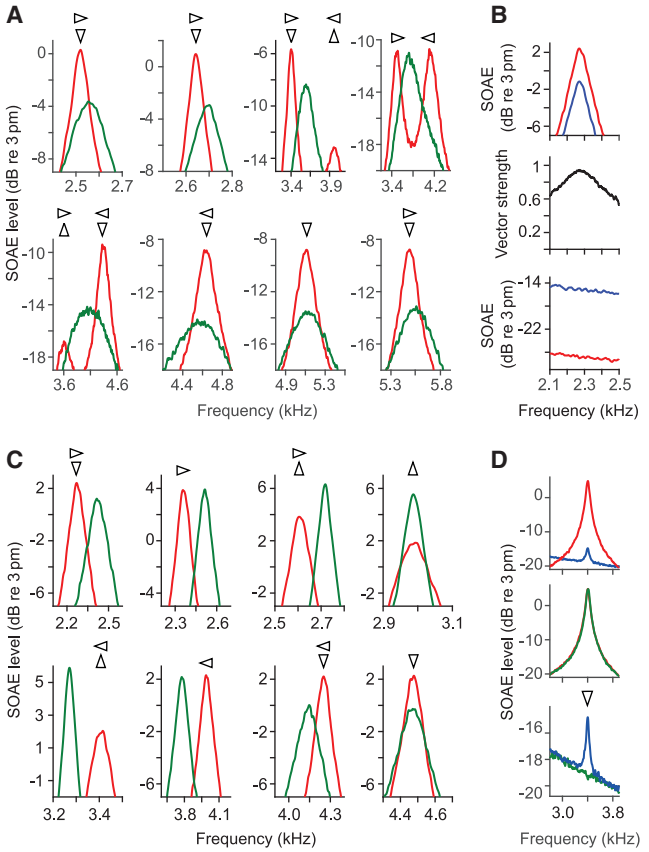

FIGURE 3 Effects of a static force load on active oscillators. Model: (*A*) an oscillator was suppressed by applying a static force equivalent to an external pressure of +600 Pa. Changes in the emission level are identified by upright and inverted open arrowheads and frequency shifts are marked by sideways open arrowheads. The spectrum of an active oscillator (*red*) was altered when its identical contralateral counterpart was suppressed (*green*). As the oscillators' peak frequency rose, the effects of suppression changed. First row, left to right: $TS = 2$, 1.9, 1.45, 1.413. Second row, left to right: $TS = 1.37$, 1.32, 1.25, 1.2. (*B*) (*Top*) Spontaneous oscillations of an active oscillator (*red*) entrained a passive oscillator (*blue*). (*Middle*) The vector strength indicated entrainment around the peak frequency. (*Bottom*) Applying an external static pressure to the active oscillator eliminated oscillations of both oscillators. Passive oscillator, $TS = 20$; active oscillator, $TS = 2$ and $K = 0.7\ K_H$. (*C*) When an active oscillator (*red*) drove a passive oscillator, the active oscillator's response to suppression of the passive oscillator (*green*) depended on the peak frequency. First row, left to right: $TS = 2$, 1.95, 1.8, 1.63. Second row, left to right: $TS = 1.5$, 1.355, 1.3, 1.255. (*D*) (*Top*) The passive oscillator's (*blue*) effect on the active oscillator (*red*) was reduced by lowering its displacement-scale parameter *DS*. (*Middle*) Suppression of the passive oscillator (*green*) had little effect on the active oscillator. (*Bottom*) Suppression of the active oscillator (*green*) eliminated emissions from both oscillators. Passive oscillator, $TS = 20$ and $DS = 0.05$; active oscillator, $TS = 1.45$ and $K = 0.7\ K_H$.

RESULTS

A model of acoustically coupled, noisy nonlinear oscillators

The detection of sound by tetrapods relies on the active process of hair cells, whose mechanosensitive hair bundles not only respond to deflections evoked by sound energy but also enhance their oscillations through active movements (33,34). Each hair bundle acts as a nonlinear oscillator whose dynamics is determined by its operating point (12,26,35); over a specific range of operating points, the bundle exhibits enhanced sensitivity and frequency selectivity (36). Under appropriate conditions, an unstimulated bundle can exhibit spontaneous oscillations that might underlie SOAEs (37).

To describe the synchronization of binaural emissions, we developed a mathematical model of two acoustically coupled, nonlinear oscillators. In this model, each eardrum was driven by a noisy nonlinear oscillator based on active hair-bundle dynamics (12,36). We assumed that the vibrations of an eardrum created not only ipsilateral SOAEs but also sound waves that traversed the mouth and caused a pressure difference across the contralateral tympanum; this provided acoustic coupling between the eardrums (Fig. 1, *C* and *D*). Propagation of the sound wave was governed by the damped-acoustic-telegraph equation (38). The ensuing displacements of each eardrum were then used to calculate the corresponding SOAEs. For simplicity, we considered the phase-locking behavior of only one pair of binaural oscillators.

Binaural correlation of SOAE spectra

Our modeling indicated that coupling of identical active oscillators to the air-filled mouth and to each other increased the peak oscillation amplitudes and reduced the peak frequencies and bandwidths (Fig. 2 *A*). To quantify the degree of synchronization between the oscillators, we employed the vector strength, a metric for which a value of zero implies no phase-locking and a value of one implies perfect phase-locking. The maximal vector strength occurred at the oscillation frequency, indicating synchronization. The vector strength also exhibited a broad peak near the fundamental frequency of the cylindrical cavity, 3.7 kHz in the model, despite no evidence for emission peaks at that frequency. In contrast, uncoupled oscillators with identical oscillation frequencies were not synchronized. These results implied that ears should be considered strongly coupled at a particular frequency only if both ears exhibited emission peaks with high vector strength at that frequency. In this work, we defined synchronized emissions as those with identical frequencies and a vector strength exceeding 0.3.

We controlled the peak frequencies of both oscillators by adjusting a timescale parameter. Owing to the acoustic coupling, the emission spectra were bimodal when the peak frequency was close to the fundamental frequency of the cavity (Fig. 2 *B*). For oscillation frequencies below the fundamental frequency, the motions of the two ends of the cavity, each representing an eardrum, were out of phase: as one eardrum moved toward the midline, the other moved away (Fig. 2 *C*). At higher frequencies, the eardrums moved in phase, a motion consistent with the second harmonic of a closed, air-filled cylindrical cavity, in which the pressures at both ends of the cavity oscillate in phase.

The SOAE spectra recorded from a gecko's ear featured several peaks at frequencies ranging from 0.5 to 5.5 kHz (Fig. S1). Comparison of the binaural spectra revealed that some emission peaks occurred at identical frequencies: their center frequencies differed by less than 10 Hz, the frequency resolution of the finite-time Fourier transform (Figs. 2 *D* and S2). The cross-correlation coefficient between the binaural spectra most often approached unity between 2 and 4 kHz, indicating spectral similarity (Fig. S3).

Investigation of the temporal correlations between the SOAEs of the two ears revealed that binaural emissions could exhibit a high degree of phase-locking over a broad frequency range. The vector strength displayed several peaks at frequencies corresponding to those of the emissions from both ears (Fig. 2 *D*). Peaks of high vector strength were associated primarily with identical-frequency SOAEs. According to our model, this observation signified strong coupling between the ears.

Analysis of the emissions recorded from 20 geckos revealed that identical-frequency peaks occurred only between 1.5 and 4.5 kHz (Fig. 2 *E*). Identical SOAE frequencies were not always associated with phase-locking, however, because some possessed low vector strengths. In these instances, the ears coincidently oscillated at similar frequencies but were not strongly coupled. In contrast, we occasionally observed high vector strengths for frequencies at which an emission apparently lacked a contralateral counterpart of the same frequency. Such a counterpart might have been excluded, however, by our conservative criterion for defining peaks as having identical frequencies.

The phase difference between most strongly coupled binaural emissions was 0.5 cycles for frequencies below 3 kHz and nil for frequencies above 4 kHz (Fig. 2, *D* and *F*). In agreement with the model, the frequency dependence of the phase difference could be explained by a fundamental frequency of the oral cavity of 3–4 kHz (Fig. 2 *C*).

Pressure dependence of SOAEs

Our model suggested that the emissions from one oscillator would change upon suppression of the identical contralateral oscillator by the imposition of an external static pressure (Fig. 3 *A*). As the static force load shifted the contralateral oscillator into the quiescent region of its state space, its spontaneous oscillations declined (12). This treatment often attenuated the emission level of the other oscillator. Depending on the oscillation frequency, the emission peaks of the unsuppressed oscillator increased or decreased in amplitude and frequency. Below ∼5 kHz, the emission peaks shifted toward the oral cavity's fundamental frequency of 3.7 kHz when the contralateral oscillator was suppressed.

Some emissions might be described adequately by one active oscillator driving a passive contralateral oscillator. Therefore, we modeled one oscillator as active and the other as passive. To ensure that the passive oscillator's displacements were similar in magnitude to those of the system of two active oscillators, we increased the compliance of the passive oscillator by raising its timescale parameter. In this case, the active oscillator drove emissions emanating from both ends of the cylindrical cavity. Suppression of

the active oscillator caused the emissions to vanish from both ears (Fig. 3 *B*). Suppression of the passive oscillator shifted the frequency and modulated the amplitude of emissions from the active oscillator (Fig. 3 *C*). At some frequencies and when the displacement of the passive oscillator was sufficiently small, however, suppression of the passive oscillator had little effect on the active one (Fig. 3 *D*).

To experimentally investigate the effects of contralateral suppression of SOAEs, we used a plastic syringe connected to the microphone coupler to control the static pressure within each ear canal (Fig. 1 *B*). All emissions were attenuated with an increase or decrease in the ear-canal pressure (Fig. S4). Suppression was typically achieved as the pressure exceeded +600 Pa to +800 Pa, a level at which the emission spectra approached the noise floor (Fig. 4).

Suppression or substantial attenuation of emissions altered the SOAE spectrum recorded from the ear contralateral to the pressure change (Figs. 4, *A* and *B* and S5). The frequency and amplitude of an emission rose, fell, or were invariant upon suppression of the contralateral ear. Consistent with the emissions generated in the model of two active oscillators (Fig. 3 *A*), we occasionally encountered SOAE peaks that were detectable only in the presence of the emissions from both ears and vanished upon suppression of the emission from either (Fig. 4 *C*). These SOAEs typically exhibited a very high vector strength.

By comparing the emission amplitudes obtained before and during suppression of the contralateral SOAEs, we tested the statistical significance of the changes in emission spectra. The SOAE level exhibited significant changes ($p < 0.001$ by Student's *t*-test) in response to suppression of the contralateral emissions (Fig. S6).

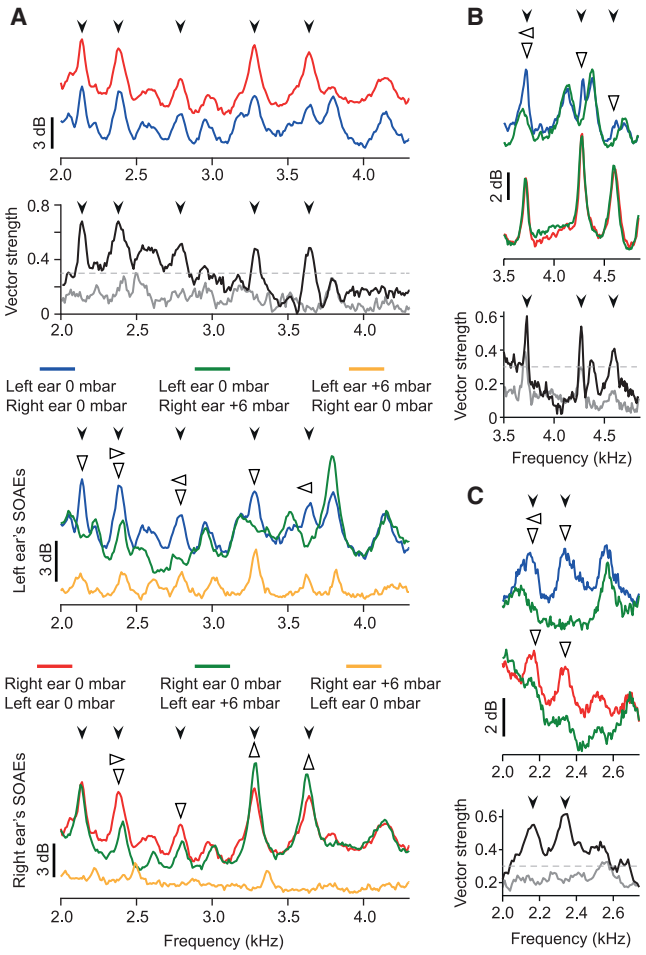

FIGURE 4 Effects of ear-canal pressure on SOAEs. Experiment: (*A*) (*top*) SOAEs were recorded from the left ear (*blue line*) and the right ear (*red line*) when both ear canals were at atmospheric pressure. (*Second*) The vector strengths of most identical-frequency SOAEs were relatively high (*black line*) and diminished when the emissions from either ear were suppressed (*gray line*). (*Third*) SOAE spectra were recorded from the left ear as the pressure was raised to +600 Pa in the right ear canal (*green line*) or in the left ear canal (*orange line*). (*Bottom*) SOAE spectra were recorded from the right ear when the pressure was adjusted to +600 Pa in the left ear canal (*green line*) or the right ear canal (*orange line*). Changes in the emission level are identified by upright and inverted open arrowheads, and frequency shifts are marked by sideways open arrowheads. Black arrowheads indicate identical-frequency SOAEs whose vector strength exceeded 0.3. (*B* and *C*) (*Top*) For two animals, the top panels illustrate emission spectra recorded from the left ear when the right ear canal was at atmospheric pressure (*blue line*) or at +600 Pa (*upper green line*). (*Middle*) SOAEs from the right ear were recorded when the left ear canal was at atmospheric pressure (*red line*) or at +600 Pa (*lower green line*). (*Bottom*) The vector strengths differed before (*black line*) and after (*gray line*) the external pressure was altered.

Effect of frequency detuning on acoustically coupled active oscillators

To determine more concretely whether some emissions arose from the interaction of two active oscillators, we sought changes in their synchronization as we increased their frequency detuning. We introduced detuning by raising the peak frequency of the left oscillator in our model while maintaining that of the right oscillator at a constant value. The peak amplitude of and entrainment between the two oscillators rose as their frequency detuning declined (Fig. 5 *A*). As a clear indication of synchronization between the active oscillators, the peak frequency of the right oscillator shifted toward that of the left (Fig. 5 *B*). Over a limited range of small frequency detuning, synchronization of active oscillators was evidenced by their peak frequencies becoming identical and vector strength achieving a maximum (Fig. 5 *C*). When the oscillators were sufficiently synchronized, their peak frequencies rose at the same rate as functions of the timescale parameter. The peak frequency of the right oscillator then returned to its unperturbed value as the left oscillator's influence fell with increased detuning.

In contrast, when an active left oscillator drove a passive right oscillator, their peak frequencies remained similar for all parameter values, and the vector strength did not exhibit a maximum (Fig. 5 *D*). The intrinsic rate at which the left

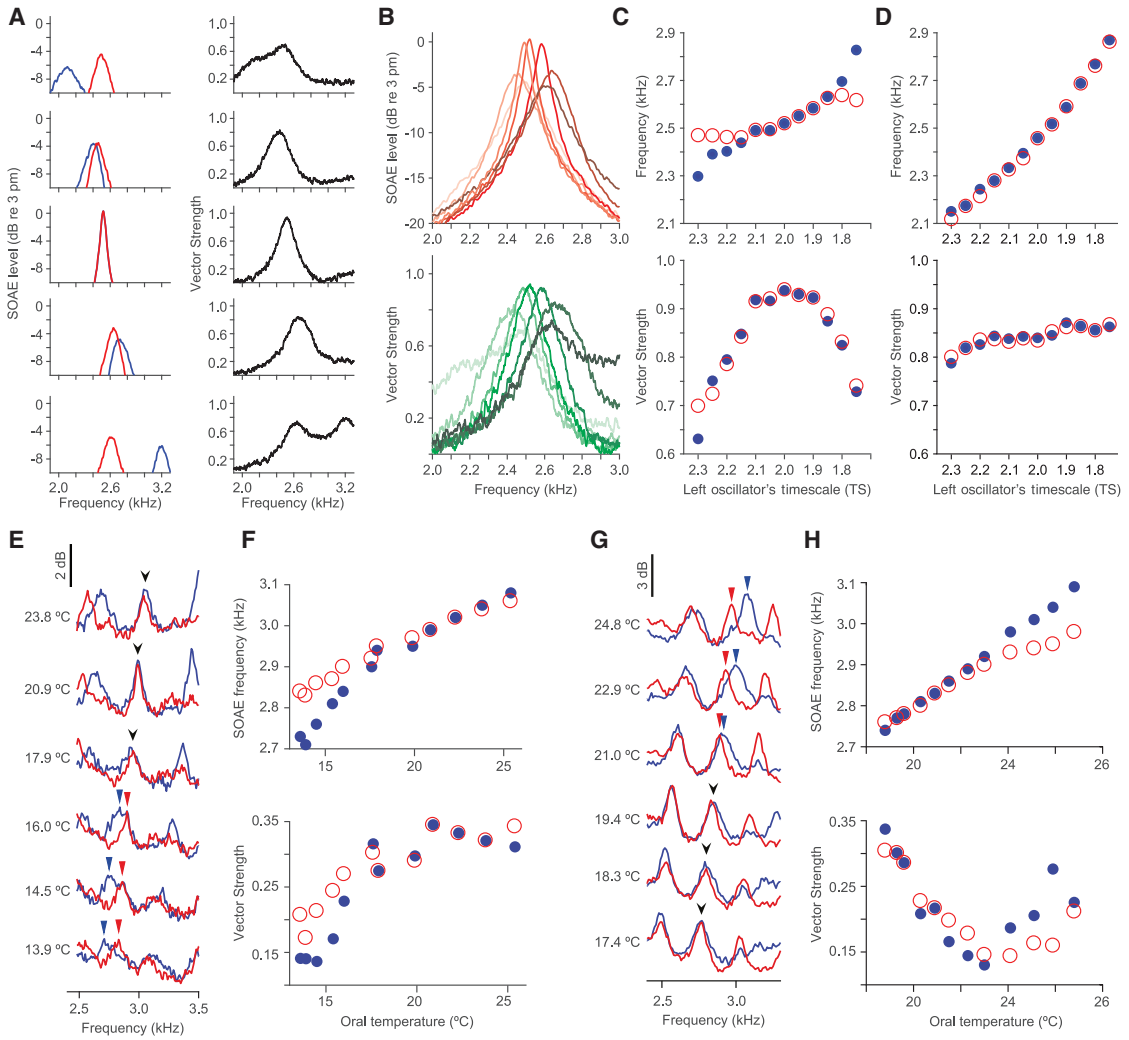

FIGURE 5 Synchronization of active-oscillator emissions. Model: (*A*) the amplitudes and vector strengths of emissions from two acoustically coupled active oscillators are shown as a function of the emission frequency for different values of the left oscillator's timescale parameter. Right oscillator (*red*), $TS = 2$; left oscillator (*blue*), top to bottom, $TS = 2.5, 2.2, 2.0, 1.8, 1.6$. (*B*) The spectral amplitude of the right unperturbed oscillator and the vector strength are shown as functions of frequency. Light to dark: $TS = 2.5, 2.2, 2.1, 2.0, 1.9, 1.8, 1.6$. (*C*) The peak emission frequency and vector strength at the peak frequency are shown as functions of the left oscillator's timescale parameter (left oscillator, *blue dots*; right oscillator, *red circles*). (*D*) The peak emission frequency and vector strength at the peaks are shown as functions of the active left oscillator's timescale parameter when the right oscillator was passive (left oscillator, *blue dots*; right oscillator, *red circles*). Right oscillator: $TS = 20$. Experiment: (*E*) SOAEs were recorded simultaneously from the left ear (*blue lines*) and right ear (*red lines*) at various temperatures of the left ear. As the temperature was reduced, a pair of identical-frequency SOAEs at 3 kHz (*black arrowheads*) separated into two nonoverlapping emission peaks (*blue arrowheads* for left ear and *red arrowheads* for right ear). (*F*) The frequencies and vector strengths of SOAE peaks from the left ear (*blue dots*) and the right ear (*red circles*) are shown as functions of the left ear's temperature. (*G*) In another animal, cooling caused two distinct SOAE peaks (*blue* and *red arrowheads*) to converge into a pair of identical-frequency SOAEs (*black arrowheads*). (*H*) The frequencies of the SOAE peaks converged and the vector strengths increased as the temperature declined.

oscillator's frequency rose was relatively insensitive to the value of the timescale parameter and was on average greater than when both oscillators were active.

Temperature dependence of SOAEs

Because previous studies revealed that the frequency of SOAEs from amphibians and reptiles depends strongly on body temperature (3,8,39), establishing a temperature difference between the two ears can be used to test the effect of detuning on acoustically coupled SOAEs. We confirmed experimentally that all SOAE peaks displayed negative shifts in frequency upon a reduction in temperature (Fig. S7). The magnitude of the shift increased monotonically as a function of the emission frequency and could be described empirically by an exponential function (39). We took advantage of this feature by reducing the local temperature of one inner ear with a cooling probe inserted into the oral cavity and pressed against the mucosa overlying the temporal bone. As the left inner ear was cooled, the right

ear's temperature also decreased owing to thermal conduction, but the magnitude of the contralateral effect was significantly smaller (Fig. S8). We were thus able to impose asymmetrical cooling on the two inner ears and to investigate the resulting effects on binaural emissions.

Asymmetrical reductions in temperature showed that a pair of synchronized emissions could separate into two weakly correlated emissions with distinct frequencies (Fig. 5 *E*). Over a moderate range of temperature changes at the left ear, these identical-frequency SOAEs underwent similar frequency shifts (Fig. 5 *F*). Below some critical temperature, however, the emissions changed at different rates with respect to the left ear's temperature, which led to their dissociation into two distinct SOAEs. The separation of emissions was concomitant with a decrease in the vector strength. Reducing the temperature also allowed some uncorrelated SOAEs to converge (Fig. 5 *G*). As the temperature decreased, the emissions first aligned in frequency before they became synchronized (Fig. 5 *H*). These observations accorded with the model's behavior when both oscillators were active and consequently implied that some emissions arose from the synchronization of two active ears.

Because emissions from both ears exhibited changes in frequency as one ear was cooled, we investigated the temperature dependence of both SOAE spectra in more detail. When the left ear was cooled, binaural SOAE spectra revealed that most emissions from that ear exhibited greater changes in frequency than did those from the right ear (Fig. 6 *A*). However, some highly phase-locked identical-frequency SOAEs observed in the left ear showed significantly smaller shifts than the neighboring peaks (Fig. 6 *B*). Some highly synchronized emission peaks from the right ear likewise underwent unusually large frequency shifts. The different temperature sensitivities of neighboring peaks occasionally led to their crossing or coalescence.

Because the temperature dependence of each SOAE frequency was approximately linear (Fig. 6 *B*), the temperature sensitivity of each peak could be quantified as the rate of change of the peak frequency with respect to the left ear's temperature. For weakly phase-locked peaks, the temperature sensitivity increased exponentially as a function of the original SOAE frequency at 24.9°C (Fig. 6, *C* and *D*). The exponential increase with emission frequency defined the intrinsic temperature sensitivity of each ear. Because

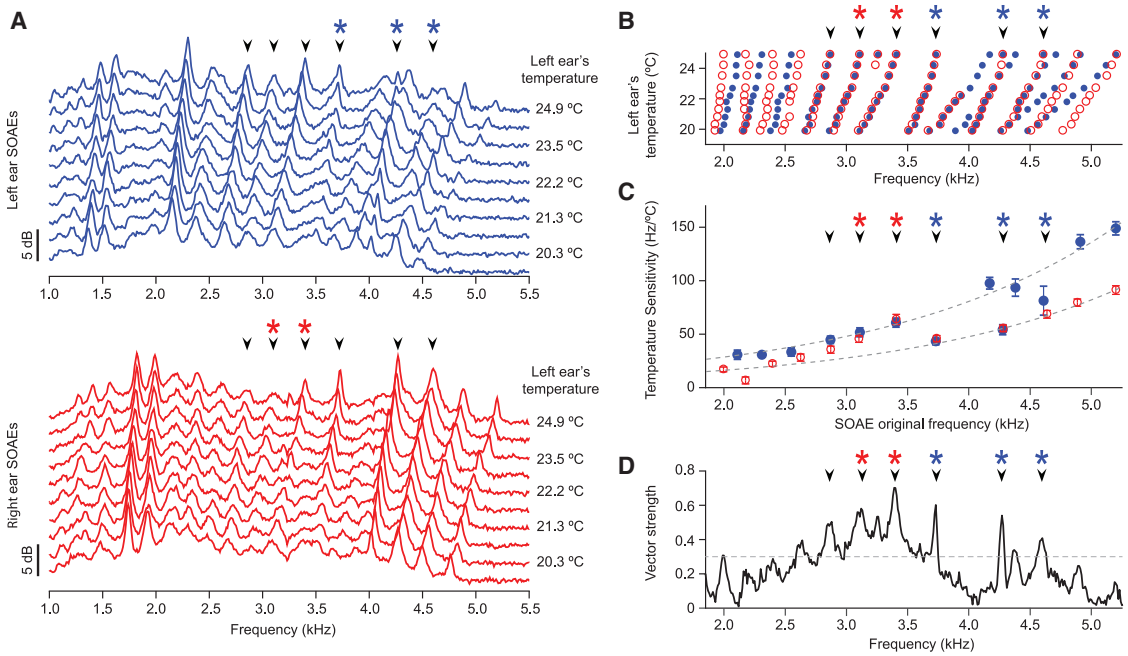

FIGURE 6 Asymmetric thermal manipulation of SOAEs. Experiment: (*A*) the spectra of SOAEs from the left ear (*blue lines*, *top panel*) and the right ear (*red lines*, *bottom panel*) were recorded as the left ear was cooled. The temperature adjacent to the left inner ear is indicated to the right of each plot. The data were obtained from the same animal as that for Figs. 2 *D* and 4 *B*. (*B*) The center frequencies of all SOAE peaks from the left ear (*blue dots*) and right ear (*red circles*) showed systematic shifts to lower frequencies during cooling. (*C*) The center frequencies of SOAEs from the left ear (*blue dots*) and right ear (*red circles*) displayed distinct sensitivities to the temperature of the left ear. The temperature sensitivities are the inverse of the line slopes in (*B*) and define the peak frequencies as a function of the left ear's temperature. Error bars indicate the 95% confidence intervals of the fits. After exclusion of identical-frequency SOAEs with high vector strength, the intrinsic temperature sensitivities of each ear could be described by the exponential functions (*gray dashed lines*): $df/dT = 9.933e^{f_0/1917}$ (*left ear*) and $df/dT = 5.303e^{f_0/1832}$ (*right ear*). f_0 denotes the original SOAE frequency at 24.9°C. The temperature sensitivities of some identical-frequency SOAE peaks in the left ear (*blue asterisks*) deviated from the intrinsic exponential curve and equaled those of their counterparts in the right ear. Certain peaks in the right ear (*red asterisks*) exhibited deviant temperature sensitivities that accorded with those of their contralateral counterparts. (*D*) The vector strengths of SOAEs at 24.9°C indicate that the peaks exhibiting deviant frequency responses were highly phase-locked. In all panels, black arrowheads label the identical-frequency SOAEs whose vector strength exceeded 0.3.

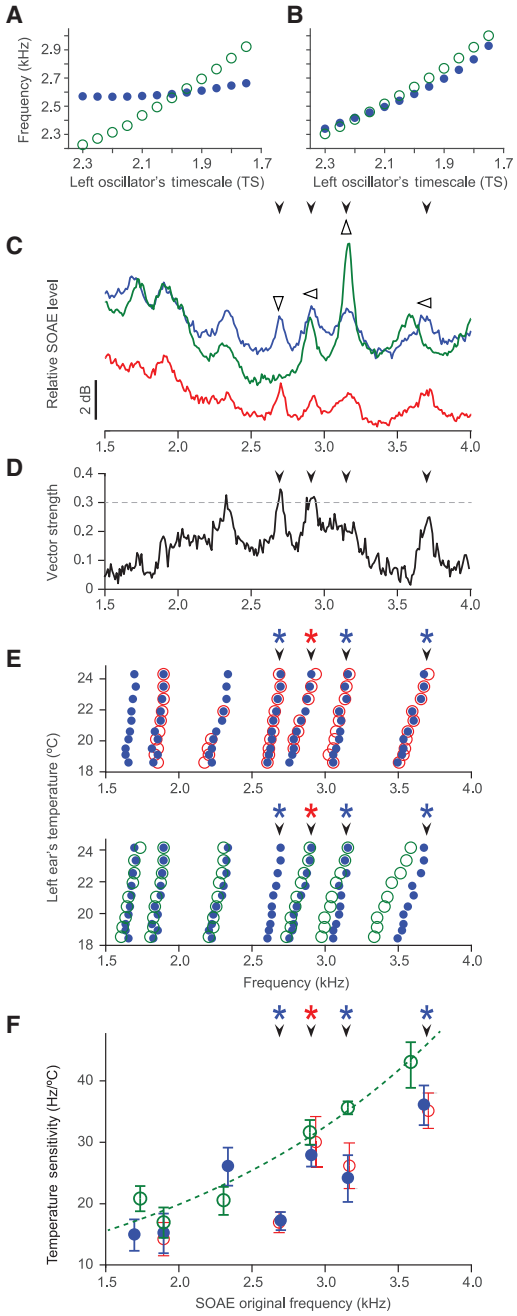

FIGURE 7 Influence of the contralateral ear on the parameter dependence of SOAEs. Model: (*A*) because the stronger right oscillator ($DS = 2$) dominated and entrained the left oscillator, the left oscillator's emission frequency changed little as its timescale parameter was altered (*blue dots*). When the right oscillator is immobilized by raising its stiffness ($K = 10\ K_H$), the left oscillator's emission frequency changed at its intrinsic sensitivity to the left timescale parameter (*green circles*). (*B*) When the right oscillator was weaker than the left oscillator ($DS = 2$), the left oscillator's sensitivity to its timescale parameter was almost independent of whether the right oscillator was immobilized (*green circles*, $K = 10\ K_H$) or not (*blue dots*). Experiment: (*C*) after recording of control SOAEs from the left ear (*blue line*) and right ear (*red line*), we suppressed the right ear's emissions by immobilizing the columella. Some emissions from the left ear (*green line*) then displayed qualitative changes (*open arrowheads*). (*D*) A plot of vector strength reveals that not all identical-frequency SOAEs sensitive to contralateral suppression exhibited vector strengths exceeding 0.3. In (*C*)–(*F*), black arrowheads label the identical-frequency SOAEs that are sensitive to contralateral suppression. (*E*) The frequencies of some SOAE peaks shown in panel C for the left ear (*blue dots*) and the right ear (*red circles*) displayed similar sensitivities to the temperature of the left ear (*asterisks*). After immobilization of the right columella, some of the left ear's emissions changed their dependence on temperature (*green circles*). (*F*) Before immobilization, the temperature sensitivity of a peak from the right ear deviated from the intrinsic sensitivity of that ear (*red asterisk*) and the left ear's temperature sensitivities did not rise monotonically with the emission frequency. Upon immobilization of the right columella, the temperature sensitivities of the left ear's emissions increased monotonically with the emission frequency (*green circles*). The left ear's peaks with originally deviant temperature sensitivities either vanished or rose to agree with that ear's intrinsic temperature sensitivity (*blue asterisks*).

the left ear's temperature was changed directly, the temperature sensitivities of weakly phase-locked emissions from that ear exceeded those of the right ear. In contrast, the temperature sensitivities of some highly synchronized peaks equaled those of the contralateral ear, a phenomenon that was observed for multiple geckos (Fig. S9). The temperature sensitivities of highly synchronized emissions deviated from the intrinsic sensitivity curve of each ear.

To understand why emissions sometimes followed the temperature sensitivity of the ipsilateral ear and sometimes that of the contralateral ear, we implemented a model in which the left oscillator was weaker than the right (Fig. 7 *A*). Because the right oscillator dominated and entrained the left, the left oscillator's emission frequency was insensitive to the value of its timescale parameter. When the right oscillator was then immobilized by increasing its stiffness substantially (12), the left oscillator's sensitivity to its timescale parameter was restored. In contrast, if the left oscillator was more robust than the right, immobilizing the right oscillator had little effect on the left oscillator's sensitivity to changes in its parameter value (Fig. 7 *B*).

To experimentally suppress emissions by increasing an eardrum's stiffness, we applied cyanoacrylate tissue adhesive at the base of the columella of the right ear, near its insertion onto the inner ear. As a result, some emissions vanished whereas others grew in magnitude and shifted in frequency (Fig. 7, *C* and *D*). These effects were similar to those obtained from increasing the ear-canal pressure.

Before suppression, the temperature sensitivity of the left ear's emissions did not rise monotonically with frequency (Fig. 7, *E* and *F*). When we cooled the left ear after immobilization of the right columella, however, the temperature sensitivity increased monotonically. For the left ear, the temperature sensitivities of peaks that were previously close to those of the right ear grew to match the temperature sensitivities of the weakly phase-locked emissions.

The model allowed us to interpret even these complex results. Two of the left ear's peaks with temperature sensitivities close to those of the right ear were the result of

strong emissions from the right ear dominating weaker emissions from the left. Another emission that vanished upon immobilization of the right ear was created by the right ear driving the left, which did not oscillate spontaneously at that frequency. Finally, one emission peak resulted from the left ear driving the weaker right ear because its temperature sensitivity was minimally affected by suppression of the right ear's emission.

Modeling the effects of interaural coupling on active sound localization

It is thought that acoustic coupling of the ears through the oral cavity allows a tokay gecko to localize sounds of wavelengths exceeding the animal's head size (40). Because the detection of directionality has been explored for only high sound levels, at which the ear's active process has little effect, it is unclear whether spontaneous activity can enhance the localization of weak sound sources (16). To investigate this issue, we analyzed the response of the model to external stimuli. Both oscillators were stimulated with external sinusoidal pressure signals of the same frequency and magnitude. We assumed that the sound source was adjacent to one ear; to account for the gecko's head size, we delayed the signal to the contralateral ear by 50 μs.

Even when the oscillators were identical, their responses to an external signal, measured at the stimulus frequency, depended on the sound source's location (Figs. 8 and S10). When the source was adjacent to the left oscillator and the stimulus frequency lay below the oscillators' emission frequency, the response of the left oscillator was smaller than that of the right oscillator. The converse was true for stimuli with frequencies above the emission frequency. Because the responses of each ear differed, the system could in principle determine the sound source's location (Fig. 8 *A*). Lessening the activity of both ears by reducing τ (12), however, decreased the maximal response of each ear (Fig. 8 *B*). The system's ability to locate the sound source could be quantified using the amplitude difference between the two ears, also known as the interaural vibration-amplitude difference (41). Activity changed the frequency dependence of this difference (Fig. 8 *C*). The difference in the bilateral response was more pronounced when the oscillators were not identical. Near the peak emission frequency of an oscillator, the size of the contralateral oscillator's response depended on the location of sound source (Figs. 8 *D* and S10). A decline in activity reduced the response amplitudes and the magnitude of the interaural difference (Fig. 8, *E* and *F*). The interaural difference of the system with reduced activity depended weakly on the stimulus frequency and on the location of the sound source. These results suggest that the acoustical coupling of active ears can allow an animal to determine the location of weak sounds.

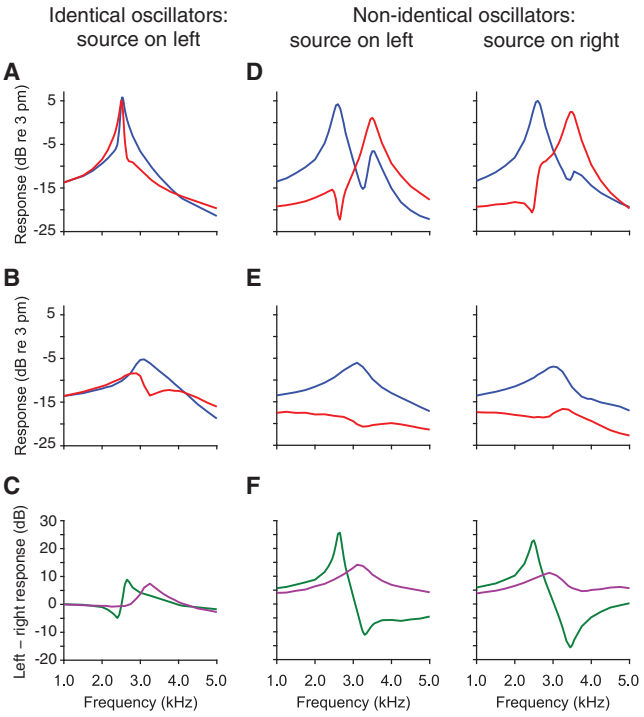

FIGURE 8 Sound source localization by acoustically coupled active oscillators. Model: (*A*) responses of identical oscillators ($TS = 2$) at the stimulus frequency are shown as functions of the stimulus frequency. (*B*) The frequency responses of identical oscillators with reduced activities are shown. (*C*) The difference between the left and right oscillators' responses measures the system's ability to locate the sound source (*green*). The frequency dependence of this interaural difference in vibration amplitude changed when the oscillators' activity was reduced (*purple*). (*D*) The response at the stimulus frequency is shown when the source was adjacent to either the left oscillator ($TS = 2$) or the right oscillator ($TS = 1.5$). (*E*) The frequency responses of the nonidentical oscillators are shown in the case of reduced activities. (*F*) The interaural difference depended on the sound source's location (*green*). Reducing activities decreased the interaural difference's magnitude, frequency sensitivity, and dependence on source location (*purple*). In the model system, a 20 dB SPL sound source was adjacent to one oscillator. To account for the travel time around the head to the other oscillator, the unattenuated signal at the contralateral oscillator was delayed by 50 μs. The responses of the left oscillator are shown in blue, and those of the right oscillator in red. An oscillator's activity was reduced by setting $\tau_j = 1$ TS.

DISCUSSION

We observed synchronization between the binaural SOAEs recorded simultaneously from the ears of the tokay gecko. Manipulations of one ear indicated that some SOAEs strongly influenced the emissions of similar frequencies from the contralateral ear. In some instances, these effects could be explained only by the interaction of two active oscillators. These observations thus add considerable evidence that SOAEs are produced by the ear's active process.

Unlike mammalian cochleas, the auditory organs of most lizard species—including gecko—lack efferent innervation in the high-frequency region responsible for the generation of SOAEs. Although bone conduction might couple the two

ears, the time delay and coupling strength are expected to be smaller than for acoustic coupling. Because a model of the ears as acoustically coupled active oscillators agreed well with the experimental observations, the interaural coupling observed in our experiments likely occurred at the peripheral level and stemmed from acoustic coupling between the eardrums.

In agreement with the experimental observations, our model captured the acoustic synchronization of the oscillators and the frequency-dependent phase differences between ears. The model enabled us to interpret the complex alterations in emission upon suppression of the contralateral ear by static pressure and the change in emission frequency as the peak frequency of the contralateral oscillator was varied. Modeling also implied that the synchronization of emissions depended on the detuning in their peak frequencies and the emission strengths of both ears. The model predicted that increases in stiffness and raising or lowering the constant force created by static pressure suppressed spontaneous oscillations in the ear (12). That these predictions have been confirmed experimentally for individual hair bundles (36,42) and now at the whole-organ level provides compelling evidence that some SOAEs arise from the spontaneous oscillations of hair bundles.

SOAEs might be generated by clusters of oscillators with a range of natural frequencies (43,44). In contrast, standing waves in the mammalian cochlea have been proposed as an explanation for SOAEs (45). Despite anatomical differences that have led to different proposals for the mechanism of SOAE generation, the emissions share numerous features across species (46,47). Here, we show that considering an emission from each ear as arising from a single active oscillator is sufficient to describe our observations. Some characteristics of SOAEs are evidently independent of the detailed mechanisms underlying their production.

Because the spontaneous activity of the two inner ears of a lizard can be synchronized, the active process of each ear affects the dynamics of both. Although internally coupled ears are thought to encode the location of high-intensity sound sources through the motions of two acoustically coupled eardrums, this effect has not been investigated for weak sounds (16–18). Our mathematical model predicts that the activities of both ears dictate the sensitivity of the system to weak sounds and consequently determine how the ears encode the location of a sound source. The frequency response and interaural difference depend on the location of the sound source, but these dependencies decline as the activity is reduced. The two ears of a gecko evidently function together as a single active system that is sensitive to the location of weak sound sources.

SUPPORTING MATERIAL

Supporting Material can be found online at https://doi.org/10.1016/j.bpj.2019.02.032.

AUTHOR CONTRIBUTIONS

Y.R. designed the experiments, conducted physiological recordings, and wrote the manuscript. D.Ó.M. carried out the theoretical analysis and modeling and wrote the manuscript. A.J.H. designed the experiments, supervised the research, and wrote the manuscript.

ACKNOWLEDGMENTS

We thank Brian Fabella for assistance with the measurement apparatus and software. A.J.H. is an Investigator of Howard Hughes Medical Institute.

SUPPORTING CITATIONS

References (48–51) appear in the Supporting Material.

REFERENCES

1. Ohyama, K., H. Wada, …, T. Takasaka. 1991. Spontaneous otoacoustic emissions in the guinea pig. *Hear. Res.* 56:111–121.
2. van Dijk, P., P. M. Narins, and J. Wang. 1996. Spontaneous otoacoustic emissions in seven frog species. *Hear. Res.* 101:102–112.
3. Manley, G. A., L. Gallo, and C. Koppl. 1996. Spontaneous otoacoustic emissions in two gecko species, Gekko gecko and Eublepharis macularius. *J. Acoust. Soc. Am.* 99:1588–1603.
4. Taschenberger, G., and G. A. Manley. 1997. Spontaneous otoacoustic emissions in the barn owl. *Hear. Res.* 110:61–76.
5. Manley, G. A. 2001. Evidence for an active process and a cochlear amplifier in nonmammals. *J. Neurophysiol.* 86:541–549.
6. Köppl, C., and G. A. Manley. 1994. Spontaneous otoacoustic emissions in the bobtail lizard. II: interactions with external tones. *Hear. Res.* 72:159–170.
7. Long, G. R., A. Tubis, and K. L. Jones. 1991. Modeling synchronization and suppression of spontaneous otoacoustic emissions using Van der Pol oscillators: effects of aspirin administration. *J. Acoust. Soc. Am.* 89:1201–1212.
8. Long, G. R., P. Van Dijk, and H. P. Wit. 1996. Temperature dependence of spontaneous otoacoustic emissions in the edible frog (Rana esculenta). *Hear. Res.* 98:22–28.
9. Hauser, R., R. Probst, and F. P. Harris. 1993. Effects of atmospheric pressure variation on spontaneous, transiently evoked, and distortion product otoacoustic emissions in normal human ears. *Hear. Res.* 69:133–145.
10. van Dijk, P., B. Maat, and E. de Kleine. 2011. The effect of static ear canal pressure on human spontaneous otoacoustic emissions: spectral width as a measure of the intra-cochlear oscillation amplitude. *J. Assoc. Res. Otolaryngol.* 12:13–28.
11. van Dijk, P., and G. A. Manley. 2013. The effects of air pressure on spontaneous otoacoustic emissions of lizards. *J. Assoc. Res. Otolaryngol.* 14:309–319.
12. Ó Maoiléidigh, D., E. M. Nicola, and A. J. Hudspeth. 2012. The diverse effects of mechanical loading on active hair bundles. *Proc. Natl. Acad. Sci. USA.* 109:1943–1948.
13. Penner, M. J., S. E. Brauth, and P. J. Jastreboff. 1994. Covariation of binaural, concurrently-measured spontaneous otoacoustic emissions. *Hear. Res.* 73:190–194.
14. Braun, M. 1998. Accurate binaural mirroring of spontaneous otoacoustic emissions suggests influence of time-locking in medial efferents. *Hear. Res.* 118:129–138.
15. van Dijk, P., H. P. Wit, and J. M. Segenhout. 1989. Spontaneous otoacoustic emissions in the European edible frog (Rana esculenta): spectral details and temperature dependence. *Hear. Res.* 42:273–282.

16. Christensen-Dalsgaard, J., and G. A. Manley. 2005. Directionality of the lizard ear. *J. Exp. Biol.* 208:1209–1217.

17. Christensen-Dalsgaard, J., and G. A. Manley. 2008. Acoustical coupling of lizard eardrums. *J. Assoc. Res. Otolaryngol.* 9:407–416.

18. Christensen-Dalsgaard, J., Y. Tang, and C. E. Carr. 2011. Binaural processing by the gecko auditory periphery. *J. Neurophysiol.* 105:1992–2004.

19. Jørgensen, M. B. 1991. Comparative studies of the biophysics of directional hearing in anurans. *J. Comp. Physiol. A Neuroethol. Sens. Neural Behav. Physiol.* 169:591–598.

20. Christensen-Dalsgaard, J. 2005. Directional hearing in nonmammalian tetrapods. *In* Sound Source Localization. Springer, pp. 67–123.

21. Pikovsky, A., M. Rosenblum, and J. Kurths. 2001. Synchronization: A Universal Concept in Nonlinear Sciences. Cambridge University Press, Cambridge, UK.

22. Lynch, J. J., and R. A. York. 2001. Synchronization of oscillators coupled through narrow-band networks. *IEEE Trans. Microw. Theory Tech.* 49:237–249.

23. Ivanchenko, M. V., G. V. Osipov, …, J. Kurths. 2004. Synchronization of two non-scalar-coupled limit-cycle oscillators. *Physica D.* 189:8–30.

24. Ohno, K., T. Ogawa, and N. J. Suematsu. 2019. Competition between global feedback and diffusion in coupled Belousov-Zhabotinsky oscillators. *Phys. Rev. E.* 99:012208.

25. Vossen, C., J. Christensen-Dalsgaard, and J. L. van Hemmen. 2010. Analytical model of internally coupled ears. *J. Acoust. Soc. Am.* 128:909–918.

26. Nadrowski, B., P. Martin, and F. Jülicher. 2004. Active hair-bundle motility harnesses noise to operate near an optimum of mechanosensitivity. *Proc. Natl. Acad. Sci. USA.* 101:12195–12200.

27. Manley, G. A. 1972. The middle ear of the tokay gecko. *J. Comp. Physiol.* 81:239–250.

28. Miller, M. R. 1973. A scanning electron microscope study of the papilla basilaris of Gekko gecko. *Z. Zellforsch. Mikrosk. Anat.* 136:307–328.

29. Manley, G. A., C. Köppl, and M. Sneary. 1999. Reversed tonotopic map of the basilar papilla in Gekko gecko. *Hear. Res.* 131:107–116.

30. Köppl, C., and S. Authier. 1995. Quantitative anatomical basis for a model of micromechanical frequency tuning in the Tokay gecko, Gekko gecko. *Hear. Res.* 82:14–25.

31. Bergevin, C., N. Mhatre, and A. Mason. 2018. Comparing external tympanum vibration and spontaneous otoacoustic emissions. *AIP Conf. Proc.* 1965:130004.

32. Zar, J. H. 1999. Biostatistical Analysis. Prentice Hall, Upper Saddle River, NJ.

33. Martin, P., and A. J. Hudspeth. 1999. Active hair-bundle movements can amplify a hair cell's response to oscillatory mechanical stimuli. *Proc. Natl. Acad. Sci. USA.* 96:14306–14311.

34. Kennedy, H. J., A. C. Crawford, and R. Fettiplace. 2005. Force generation by mammalian hair bundles supports a role in cochlear amplification. *Nature.* 433:880–883.

35. Fredrickson-Hemsing, L., S. Ji, …, D. Bozovic. 2012. Mode-locking dynamics of hair cells of the inner ear. *Phys. Rev. E Stat. Nonlin. Soft Matter Phys.* 86:021915.

36. Salvi, J. D., D. Ó Maoiléidigh, …, A. J. Hudspeth. 2015. Control of a hair bundle's mechanosensory function by its mechanical load. *Proc. Natl. Acad. Sci. USA.* 112:E1000–E1009.

37. Martin, P., D. Bozovic, …, A. J. Hudspeth. 2003. Spontaneous oscillation by hair bundles of the bullfrog's sacculus. *J. Neurosci.* 23:4533–4548.

38. Till, B. C., and P. F. Driessen. 2014. A didactically novel derivation of the telegraph equation to describe sound propagation in rigid tubes. *Eur. J. Phys.* 35:015007.

39. Manley, G. A., and C. Köppl. 1994. Spontaneous otoacoustic emissions in the bobtail lizard. III: temperature effects. *Hear. Res.* 72:171–180.

40. Wever, E. G. 1978. The Reptile Ear-Its Structure and Function. Princeton University Press, Princeton, NJ.

41. Jørgensen, M. B., B. Schmitz, and J. Christensen-Dalsgaard. 1991. Biophysics of directional hearing in the frog Eleutherodactylus coqui. *J. Comp. Physiol. A Neuroethol. Sens. Neural Behav. Physiol.* 168:223–232.

42. Salvi, J. D., D. Ó Maoiléidigh, and A. J. Hudspeth. 2016. Identification of bifurcations from observations of noisy biological oscillators. *Biophys. J.* 111:798–812.

43. Vilfan, A., and T. Duke. 2008. Frequency clustering in spontaneous otoacoustic emissions from a lizard's ear. *Biophys. J.* 95:4622–4630.

44. Wit, H. P., P. van Dijk, and G. A. Manley. 2012. A model for the relation between stimulus frequency and spontaneous otoacoustic emissions in lizard papillae. *J. Acoust. Soc. Am.* 132:3273–3279.

45. Shera, C. A. 2003. Mammalian spontaneous otoacoustic emissions are amplitude-stabilized cochlear standing waves. *J. Acoust. Soc. Am.* 114:244–262.

46. Bergevin, C., D. M. Freeman, …, C. A. Shera. 2008. Otoacoustic emissions in humans, birds, lizards, and frogs: evidence for multiple generation mechanisms. *J. Comp. Physiol. A Neuroethol. Sens. Neural Behav. Physiol.* 194:665–683.

47. Bergevin, C., G. A. Manley, and C. Köppl. 2015. Salient features of otoacoustic emissions are common across tetrapod groups and suggest shared properties of generation mechanisms. *Proc. Natl. Acad. Sci. USA.* 112:3362–3367.

48. Keefe, D. H. 1984. Acoustical wave propagation in cylindrical ducts: transmission line parameter approximations for isothermal and nonisothermal boundary conditions. *J. Acoust. Soc. Am.* 75:58–62.

49. Nyquist, H. 1928. Thermal agitation of electric charge in conductors. *Phys. Rev.* 32:110–113.

50. Callen, H. B., and T. A. Welton. 1951. Irreversibility and generalized noise. *Phys. Rev.* 83:34–40.

51. Zurita-Sanchez, J. R., and C. Henkel. 2006. Lossy electrical transmission lines: thermal luctuations and quantization. *Phys. Rev. A.* 73:063825.